J Adv Ceram

Research Article

Ce:GAGG and Al_2O_3–Ce:GAGG phosphor ceramics for laser-driven lighting: Effects of Ga^{3+} substitution

Denis Yu. Kosyanov[1,2,✉], Anastasia A. Vornovskikh[1], Alexey P. Zavjalov[1,3], Zlata E. Priimak[1], Andrei A. Leonov[2], Andrei A. Obraztsov[4], Yanbin Wang[5,6], Ziqiu Chen[5,6], Zhenzhen Zhou[5,6], Jiang Li[5,6,✉]

Cite this article: Kosyanov D, Vornovskikh A, Zavjalov A, et al. *J Adv Ceram* 2026, **15**(4): 9221267. https://doi.org/10.26599/JAC.2026.9221267

ABSTRACT: Monophase $Ce:Gd_3Al_{5-x}Ga_xO_{12}$ (Ce:GAGG) with x = 0.5–3.0 and 50 vol% Al_2O_3–containing composite phosphor ceramics (PCs) were prepared in a pure oxygen atmosphere. The effects of Ga^{3+} substitution on their phase formation, microstructure, and luminescence properties were systematically investigated. For Ce:GAGG series samples, no additional phases were identified, and the distribution of Ga between the octahedral $(Al/Ga)_2$ (0, 0, 0) and tetrahedral $(Al/Ga)_3$ (0.375, 0, 0.25) sites of the garnet phase was clarified. For Al_2O_3–Ce:GAGG composites, the exchange of Al and Ga elements between the phases of garnet Ga(Al,Ga)G and oxide $(Al,Ga)_2O_3$ was revealed, and the transformation of $(Al,Ga)_2O_3$ from the α- to κ-phase ($x \geq 2.0$) with the formation of elongated grains and their partial melting (x = 3) is shown. This was also reflected in a less pronounced shift of the photoluminescence peak (PL) toward shorter wavelengths for the composite series in comparison with the monophase series: with an increase in x to 3.0, the shift in the position of the PL peak of intensity by 18 nm for Al_2O_3–Ce:GAGG was equivalent to that for Ce:GAGG at x = 1.5. A phosphorescence phenomenon was found at x = 2.5 and 3.0 for monophasic Ce:GAGG compositions. Under the excitation of 1 W 450 nm LDs in reflection mode, 0.4 mm-thick Al_2O_3–Ce:GAGG with x = 0.5–1.5 had an optimum correlated color temperature of 5400–6300 K, a luminous efficiency of 123–145 lm·W^{-1}, and a color rendering index (Ra = 69–64). The obtained PCs showed high application potential in solid-state laser lighting.

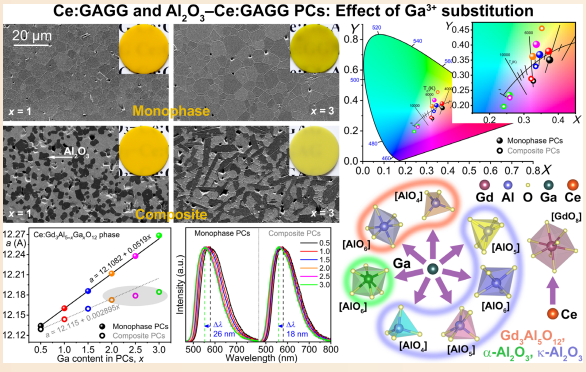

KEYWORDS: $Ce:Gd_3Al_{5-x}Ga_xO_{12}$ (Ce:GAGG); ceramic phosphors; oxygen sintering; phase formation; microstructure; luminescence performance; laser-driven lighting.

1 Introduction

Laser lighting has a number of advantages over light-emitting diode (LED) lighting in terms of producing white light with a high lumen density: low efficiency drop of blue laser diodes (LDs) with increasing current (effective input power density ~250 W·mm^{-2}); high output power and brightness, optical and high differential gain; and the ability to place the light source outside the lighting device to ensure optimal temperature conditions. Therefore, high-brightness white LDs attract increasing interest for use in automobile low- and high-beam headlights; searchlights for aircraft, underwater and surface vehicles, including unmanned types; in search and rescue operations; etc. [1,2]. However, insufficient heat dissipation by phosphors when exposed to high-power laser radiation, as well as poor quality of white light color rendering (Ra), represent key limitations hindering progress in the field of laser illumination [3].

Scientists and developers have announced many new types of thermally robust phosphors for white LDs, including phosphor in glass (PiG), composite structured PiG films (PiGF), PiGF with incorporated particles, transparent ceramics, single crystals, eutectic crystals, glass–ceramics, and composite ceramics [4–9]. It has been shown that Ce:YAG-based ceramic materials, featuring thermal conductivity in the range of 9–14 W·m^{-1}·K^{-1} along with high thermal strength and fracture toughness, can operate under high input power conditions to produce bright white light without obvious thermal quenching of photoluminescence (PL) intensity. In particular, the prospects of the strategy for the development of

[1] Far Eastern Federal University, Vladivostok 690922, Russia. [2] Institute of Automation and Control Processes, Far Eastern Branch of the Russian Academy of Sciences, Vladivostok 690041, Russia. [3] Department of Synchrotron Research of Functional Materials, Synchrotron Radiation Facility SKIF, Boreskov Institute of Catalysis, Siberian Branch of the Russian Academy of Sciences, Koltsovo 630559, Russia. [4] LLC "SPA"Telemetry", Kaluga 248010, Russia. [5] State Key Laboratory of High Performance Ceramics, Shanghai Institute of Ceramics, Chinese Academy of Sciences, Shanghai 201899, China. [6] Center of Materials Science and Optoelectronics Engineering, University of Chinese Academy of Sciences, Beijing 100049, China.

✉ Corresponding authors. E-mail: D. Kosyanov, kosianov.diu@dvfu.ru; J. Li, lijiang@mail.sic.ac.cn

Received: November 12, 2025; Revised: February 17, 2026; Accepted: February 19, 2026

composite ceramic structures based on thermostable Al_2O_3 (32–35 $W \cdot m^{-1} \cdot K^{-1}$) and luminescent Ce:YAG phases are declared. Corundum grains also serve as scattering centers (refractive indices n = 1.76 and 1.83 for α-alumina and YAG, respectively), thereby increasing the efficiency of light extraction [10]. Despite the fact that the pores (n = 1) can also act as secondary light-scattering "phases", when solving the problem of achieving a high density of incoming pumping power, their presence can be critical due to a sharp decrease in the ability of the material to remove heat [11].

However, Ce:YAG yellow phosphors (PL peak at ~540 nm) are characterized by the presence of a wide cyan cavity in the emission spectrum in the region of 460–520 nm due to the ultranarrow (~2 nm) emission band of the blue LD [12,13]. In addition, the insufficient contribution of the longwave (red) component makes it impossible to achieve full-color illumination. As a result, incorrect display of the real color of objects limits the applicability of these phosphors for many promising applications. The presence of high Ra is possible only in the case of a balanced spectral distribution over the entire visible region, ensuring high FWHM (full width at half maximum) values and expanding the blue emission region [13–15].

For Ce^{3+}-doped garnets, an increase in the radius of the matrix cation in the dodecahedral position leads to splitting of the crystalline field, and as a result, the Ce^{3+} emission is shifted to the longwave region (the so-called "red" shift). On the other hand, an increase in the radius of ions occupying tetrahedral and/or octahedral positions leads to a shift of emission toward shorter wavelengths (the so-called "blue" shift). From this point of view, Ce^{3+}-doped ceramic solid solutions of the $Gd_3Al_5O_{12}$ (GAG)—$Gd_3Ga_5O_{12}$ (GGG) system seem to be promising color converters for laser-driven lighting [3,16]. The existence of GAGG is confirmed before the ratio Al/Ga—4.5/0.5; the GAG composition having the greatest cleavage of the crystalline field is thermodynamically unstable (there is a phase decay of GAG → Al_2O_3 + 3GAP) [17–19]. Additionally, the fabrication of GAGG ceramic solid solutions requires the use of oxygen or inert atmospheres due to the partial decomposition of Ga_2O_3 and the evaporation of gallium in a vacuum/reducing medium at 1300 °C [20,21].

The presented approach will obviously enrich the spectrum. However, a change in the matrix density, as well as the interaction between various active ions, can result in a decrease in quantum efficiency and a pronounced effect of thermal quenching of the PL intensity. Therefore, spectral regulation and comprehensive performance enhancement of garnet-structured Ce:GAGG phosphor ceramics (PCs) is an important task. In this study, Ce:GAGG and Al_2O_3–Ce:GAGG PCs were prepared in a pure oxygen atmosphere, and the effects of Ga^{3+} substitution on their phase formation, microstructure, and luminescence properties were systematically investigated.

2 Experimental

2.1 Obtaining PCs

The formation of oxide stoichiometry systems of monophase ceramics Ce:$Gd_3Al_{5-x}Ga_xO_{12}$ (x = 0.5, 1.0, 1.5, 2.0, 2.5, 3.0) was carried out by wet grinding of high-purity (≥ 99.99%) commercial powders α-Al_2O_3, Gd_2O_3, Ga_2O_3, and CeO_2 in ball planetary mills with subsequent stages of drying, granulation, and annealing from organic binders. The content of Ce^{3+} ions was fixed at 0.5 at%. For composite formulations of Al_2O_3–Ce:$Gd_3Al_{5-x}Ga_xO_{12}$ stoichiometry, the corundum phase content was 33 wt% (~50 vol%). SiO_2 (in the form of tetraethyl orthosilicate, 0.5 wt%) was used as a sintering additive. Compacting of powder systems was carried out in two stages: uniaxial pressing and subsequent cold isostatic pressing at 250 MPa. PCs were obtained by sintering in an oxygen atmosphere at 1600 °C and isothermal holding time of 5 h. For further studies, the samples were ground and polished on both sides to a thickness of 0.4 mm.

2.2 Characterizations

The phase composition was characterized using a diffractometer (Drone 8 X-ray, Russia) on a Cu $K\alpha_{1,2}$ doublet in the range of double angles of 15°–90° with the pitch of 0.02° and the effective accumulation time of 3 s. Quantitative analysis of the diffractograms was carried out by the Rietveld method using the open source software "FullProf Suite" [22,23] and the open source database "Crystallography Open Database (COD)" [24,25]. The garnet phase $Gd_3Al_{2.3}Ga_{2.7}O_{12}$ (COD ID 7240198) and corundum α-Al_2O_3 (COD ID 9009671) were selected as references. In addition, for samples of composites with a low Al/Ga ratio, impurity phase reflexes were present – presumably low-symmetric orthorhombic, similar to κ-Al_2O_3 or κ-Ga_2O_3; therefore, the κ-Al_2O_3 (COD ID 1000442) phase was additionally selected as a reference.

The microstructure of the ceramics was examined by a scanning electron microscope (SEM; Ultra 55+, Carl Zeiss, Germany). The average grain sizes of the constituent phases were calculated by the secant method, analyzing surface images at the same magnification (thermal etching at 1300 °C/5 h) [26].

The total transmittance over the wavelength range from 200 to 800 nm was tested by an ultraviolet–visible–near-infrared (UV–Vis–NIR) spectrophotometer (Cary 5000, Varian Medical Systems, Inc., USA). PL spectra were obtained at room temperature (RT) using a photomultiplier (R 928, Hamamatsu Photonics, Japan), covering UV–Vis–NIR wavelengths up to 830 nm. Stationary PL spectra were obtained at the maximum excitation wavelength λ_{ex} = 460 nm with a step of 1 nm and an integration time of 0.1 s. Time-resolved PL measurements were performed using the method of time-correlated single photon counting at RT with an attenuation window of 1 μs. A pulsed LED with a pulse duration of 1 ns and a wavelength of 450 nm was used to excite the PL when measuring the attenuation spectra. The values of the external quantum efficiency η(EQE) were measured using an integrating sphere mounted on a spectrofluorometer (FluoroLog-3, Horiba Scientific, Japan). Thermal conductivity was calculated using the formula $\kappa = \rho \cdot \alpha \cdot C_p$, where ρ, α, and C_p represent the actual density, thermal diffusivity and specific heat capacity, respectively. The thermal diffusivity and specific heat capacity were recorded using a laser flash apparatus (LFA467, Netzsch-Gerätebau GmbH, Germany) and a high-temperature specific heat meter (MHTC96, Setaram Instrumentation, France).

Lighting characteristics (luminous efficiency LE, color coordinates CIE, correlated color temperature CCT, and color rendering index (Ra)) were measured when excited by blue LD at an excitation wavelength (λ_{ex} = 450 nm) in the "reflection" mode. Previously, ceramic samples were glued to an aluminum radiator and tested using an integrating sphere connected to a charge-coupled spectrometer (OHSP-350, Hangzhou Hopoo Light and Color Technology Co., Ltd., China).

3 Results and discussion

3.1 Effects of Ga^{3+} substitution on the phase formation and microstructure of PCs

Figure 1 shows the appearance of Ce:GAGG and Al_2O_3–

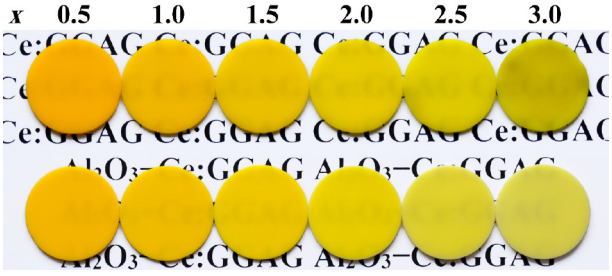

Fig. 1 Appearance of 1.0-mm-thick $Ce:Gd_3Al_{5-x}Ga_xO_{12}$ and Al_2O_3–$Ce:Gd_3Al_{5-x}Ga_xO_{12}$ PCs with different Ga contents (x = 0.5–3.0).

Ce:GAGG PCs with different Ga contents. With an increase in the level of Ga^{3+} substitution, the saturated orange-yellow hue of Ce:GAGG ceramics gradually changed to light yellow. The samples of the composites were characterized by a color several tones lower due to the lower content of Ce^{3+} ions per unit volume. These compositional inhomogeneities should be attributed to the behavior of the material with a particular composition during sintering.

The manifestation of dark regions (for Ce:GAGG) and a green shade (for Al_2O_3–Ce:GAGG) in both series at x = 2.5 and 3.0 may indicate an uneven distribution of components with the formation of phases of variable composition and the presence of defects in the crystal lattice (in particular, traps of charge carriers) acting as luminescence killer centers [27–29]. In this case, a violation of the homogeneity of the distribution of active luminescence centers and/or the formation of inactive phases will lead to degradation of the light output of the phosphor.

Figure 2 shows the diffraction patterns of both series of samples (monophase and composite phosphor ceramics, "MPCs" and "CPCs") in comparison with the model curves constructed on the basis of the reference phases from the COD database. For the Ce:GAGG series, only the garnet phase was detected, while constructing the model for the reference phase, Ce substitution was introduced, and the total stoichiometry was adjusted according to the nominal composition. The final formula was of the form $Gd_{2.985}Ce_{0.015}Al_{5-x}Ga_xO_{12}$, with a division by sites—$(Gd_{2.985}Ce_{0.015})(Al_{2-y}Ga_y)(Al_{3-z}Ga_z)O_{12}$, where $y + z = x$, and x = 0.5, 1.0, 1.5, 2, 2.5, 3.0. While maintaining the general stoichiometry, the distribution of Ga between the two sides of the garnet varied: octahedral $(Al/Ga)_2$ (0, 0, 0) and tetrahedral $(Al/Ga)_3$ (0.375, 0, 0.25). Vegard's law can be considered to be observed—noticeable deviations are detected only for a sample with x = 3 (Fig. 3(a)). The results of quantitative analysis on the value of the lattice parameter and the distribution of Ga on various sites found good agreement with the literature data: for GAGG garnet with stoichiometry of $Gd_3Al_{5-x}Ga_xO_{12}$ at x =0, 2, 3, 5 [30]; for Ce:GAGG garnet with stoichiometry of $Gd_{2.97}Ce_{0.03}Al_{2.3}Ga_{2.7}O_{12}$ (COD ID 7240198) [31]; and for YAGG garnet with stoichiometry of $Y_3Al_{5-x}Ga_xO_{12}$—at x = 0, 1, 2, 3, 4 (COD ID 2003066-2003070) [32] and at x = 1.03, 1.92 (COD ID 2107339), x = 2.9, 4.08 [33]. In the expression for Vegard's law, taking into account the occupation of various sites by Ga atoms $a = 12.1081 + 0.0517y + 0.0520z$, the coefficients turned out to be close to the values for the linear dependence $a = 12.1082 + 0.0519x$ shown in Fig. 5(a), where $x = y + z$.

For the series of Al_2O_3–Ce:GAGG PCs, with an increase in the total Ga content in the system, an increase in the lattice parameters was observed for both the garnet-type phase and for alumina. Moreover, in the Ce:GAGG phase, this dependence had a gentler appearance than for a monophasic series. This indicates the formation of a garnet phase in composites with a lower Ga content (compared to the nominal), as well as the partial replacement of Al atoms with Ga in aluminum oxide. Therefore, in the model for a series of composites, the total amount of Ga in the garnet phase was associated with the parameter of its lattice with a linear dependence obtained for a monophase series of Ce:GAGG samples (excluding the point x = 3, Fig. 3(a)). In addition to the variation in the Al/Ga ratio on the individual sides of the garnet, it also varied on the octahedral site $(Al/Ga)_2$ (0, 0, ~0.35) of α-$Al_{2-w}Ga_wO_3$ corundum, while observing the general stoichiometry according to the nominal compositions. Vegard's law for both phases in the composite series was observed up to x = 2 (Fig. 3).

It is worth paying attention to the XRD of the composite sample with x = 3 (Fig. 2). The corundum phase was not detected; however, the presence of multiple reflexes other than the reflexes of the garnet phase can be associated with a low-symmetric orthorhombic phase of the κ-Al_2O_3 type (COD ID 1000442). At x = 2.5, the reflexes of the corundum phase α-$(Al,Ga)_2O_3$ and this new phase had a comparable brightness. At x = 2, with the α-$(Al,Ga)_2O_3$ phase dominant, the brightest reflexes of the new phase were also identified. According to [34], gallium oxide Ga_2O_3 can also have at least a local structure of orthorhombic κ-phase, which in this case also suggests the formation of a κ-$(Al,Ga)_2O_3$ solid solution. It is possible that the transition with the loss of symmetry $\alpha \rightarrow \kappa$ is caused by the excessive content of Ga in the

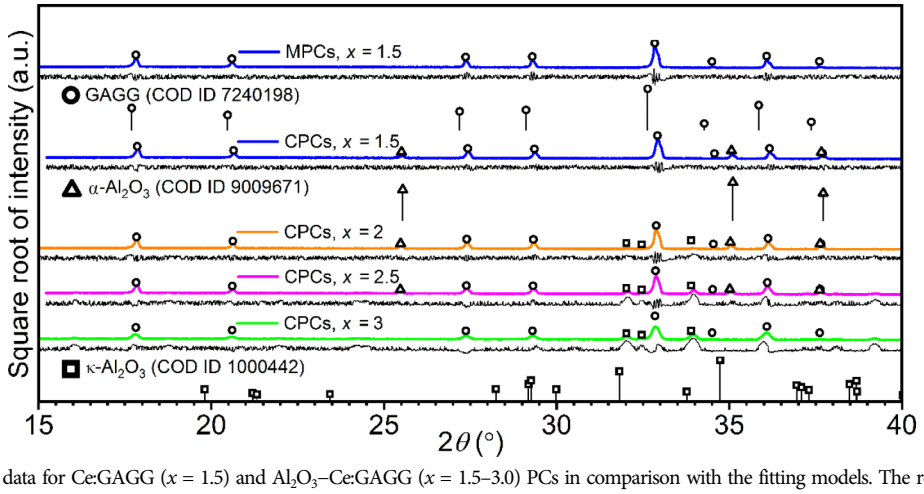

Fig. 2 Part of the XRD data for Ce:GAGG (x = 1.5) and Al_2O_3–Ce:GAGG (x = 1.5–3.0) PCs in comparison with the fitting models. The reflection positions of the reference phases are presented only for the Cu $K\alpha_1$ wavelength.

composition of the oxide $(Al,Ga)_2O_3$. This is indicated by the greater content of Ga in the κ-phase, which can be interpreted as its greater capacity and greater tolerance to introduction into the structure of larger Ga atoms due to symmetry breaking. Due to the low symmetry and the presence of many other overlapping reflexes, it was impossible to accurately determine the lattice parameters and select the Al/Ga ratios for each of the 4 different sites in the κ-phase lattice (Fig. 3). However, for x = 3, it was possible to assess the parameters of the κ-$(Al,Ga)_2O_3$ lattice by the position of its brightest reflexes (1 2 2), (0 3 1) and the relatively weak reflex accompanying them (0 1 3) superimposed on the left on the base of the main reflector of the garnet phase (4 2 0) (Fig. 2). This correlation of experimentally observed reflexes gave an estimate of the lattice parameters of this phase (a, b, c) = (5.021, 8.708, 8.856). The structures of the GAG, α-Al_2O_3, and κ-Al_2O_3 unit cells and possible ways of replacing Al with Ga are shown in Fig. 4.

The presence of a new phase made it possible to assess only the parameters of the composite phases of Ce:GAGG and α-$(Al,Ga)_2O_3$ in samples with x = 2–3. However, this required further modification of the assay procedure for composite PCs with x > 1.5. Thus, the κ-$(Al,Ga)_2O_3$ phase was not included in the model. However, instead of observing the total amount of Ga in accordance with the nominal composition, the lattice parameter $a = b$ of the α-$(Al,Ga)_2O_3$ phase, while maintaining its general stoichiometry, was associated with the content of Ga in it in accordance with the linear dependence between the actual content of Ga in its composition and its lattice parameters. This linear dependence was determined from the first three points in the series (x = 0.5–1.5) corresponding to the Ga content in the corundum composition w_α = 0.02–0.12, which was extrapolated to higher Ga content in this phase (up to w_α = 0.18 at x = 2.5). This made it possible to calculate the lack of Ga in the total composition of the main phases of the model and determine the degree of Ga substitution in the new phase (w_κ). The proportion of the new κ-$(Al,Ga)_2O_3$ phase in the total amount of $(Al,Ga)_2O_3$ oxide (Table 1) was also estimated by the molar deficiency of the α-$(Al,Ga)_2O_3$ phase in the model (compared to the nominal composition of the powder mixture).

SEM images of the surface of PCs after thermal etching are

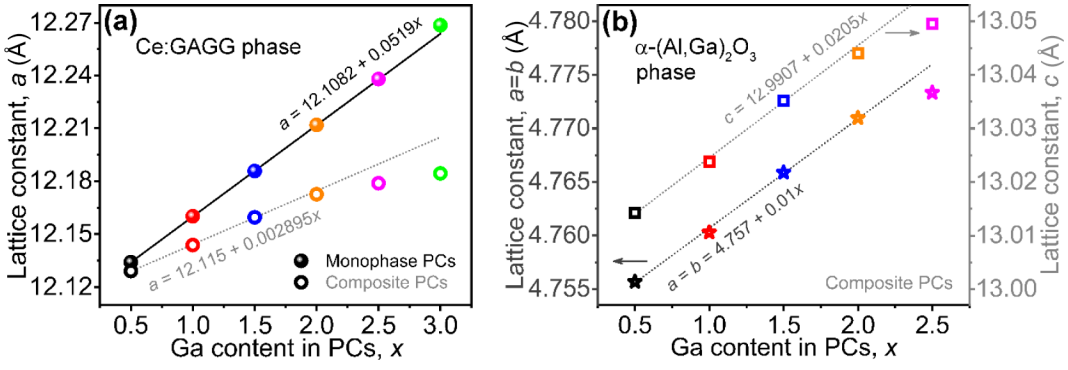

Fig. 3 Lattice parameters of (a) garnet and (b) alumina-type phases with a linear approximation of the first few points for (a) Ce:GAGG and (a, b) Al_2O_3–Ce:GAGG PCs with different Ga contents.

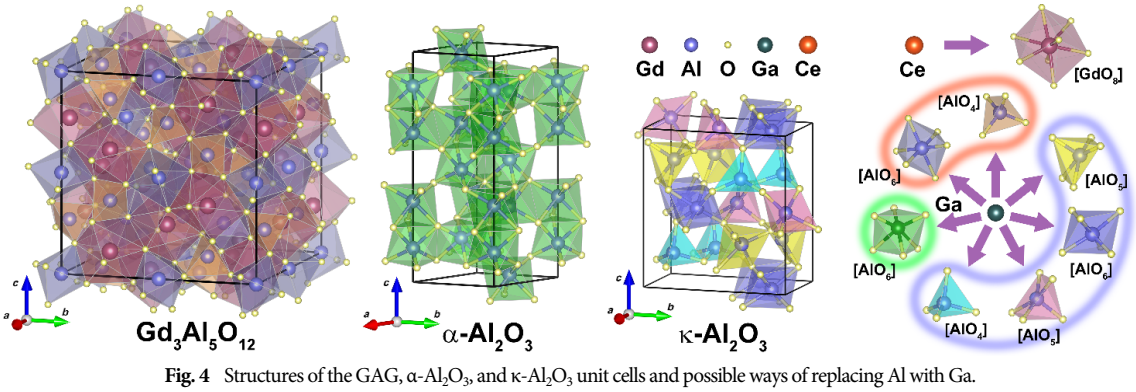

Fig. 4 Structures of the GAG, α-Al_2O_3, and κ-Al_2O_3 unit cells and possible ways of replacing Al with Ga.

Table 1 Stoichiometric coefficients in the constituent phases of PCs

Nominal Ga content	$(Gd_{2.985}Ce_{0.015})(Al_{2-y}Ga_y)(Al_{3-z}Ga_z)O_{12}$								$(Al_{2-w}Ga_w)O_3$
	Monophase serie			Composite serie					
	Octo-hedral	Tetra-hedral	Σ	Octo-hedral	Tetra-hedral	Σ	α	κ	κ
x	y	z	$y+z$	y	z	$y+z$	w_α	w_κ	(mol%)
0.5	0.15	0.35	0.50	0.13	0.27	0.40	0.02	—	—
1.0	0.21	0.79	1.00	0.14	0.55	0.69	0.08	—	—
1.5	0.43	1.07	1.50	0.18	0.81	0.99	0.12	—	—
2.0	0.56	1.44	2.00	0.27	0.97	1.24	0.15	0.28	17
2.5	0.72	1.78	2.50	0.48	0.89	1.37	0.18	0.31	60
3.0	1.00	2.00	3.00	0.84	0.64	1.48	—	0.33	100

shown in Fig. 5. The effect of Ga^{3+} substitution in Ce:GAGG on their grain structure was complex: a maximum was observed at x = 2.5 (10.3 μm), with an overall increase in average sizes in the series from 6.7 to 7.7 μm. In addition, the Ce:GAGG compositions with x = 2.5–3.0 had a significant expansion of the grain size distribution (up to 2 times compared to the compositions at x = 0.5–1) due to the presence of single grains up to 20 μm in size (Figs. 5(a)–5(c)). As shown in Figs. 5(d)–5(f), the bright part in the composite PCs is the garnet phase, while the dark part is alumina. The phase boundaries in the composite series prevented diffusion along the grain boundaries, which inhibited their growth. Thus, the "mechanism of self-limiting growth" ensured the stabilization of the average sizes of the composite phases. At the same time, as the total amount of Ga in the system increased, the dependencies of changes in the average grain size were multidirectional: an increase in the size of alumina in the range from 4.7 to 6.3 μm, with a slight decrease for garnet from 5.4 to 4.7 μm (Fig. 6). In the composite with x = 3, intensive recrystallization of alumina was observed with the formation of elongated grains and their partial melting and coalescence of pores (Fig. 5(f)). Obviously, the observed $(Al,Ga)_2O_3$ phase transition α → κ is a significant factor capable of causing these microstructural changes [29].

3.2 Analysis of the optical and luminescence properties of PCs and parameters of wLDs based on them

Figure 7(a) shows the dependence of the total transmittance at a wavelength of 800 nm on the Ga content. For monophasic Ce:GAGG formulations, some increase in values from ~25% (x = 0.5) to ~30% (x = 2.0 and 3.0) is shown. The values for the series of composites practically did not change and amounted to 21%±1% (with a single thickness of samples in the series ~0.4 mm). Figure 7(b) shows the PL spectra of ceramics in the range of λ = 480–800 nm. The wide band of emission corresponds to the transitions of the luminescence centers from the excited 5d state to the main state to the multiplet levels $^2F_{5/2}$ and $^2F_{7/2}$. With an increase in the Ga content, a shift of the PL peaks to the region of shorter wavelengths by ~26 and ~18 nm was observed with their narrowing by ~9 and ~3 nm, respectively, in the Ce:GAGG and Al_2O_3–Ce:GAGG PC series (Fig. 7(b)). These differences are associated with the peculiarities of the crystalline and electronic structure of the garnet matrix: the contribution to the splitting of the crystalline field in the garnet structure due to the replacement of Al by larger Ga atoms in the tetrahedral and/or octahedral positions is partially offset due to the formation of solid solutions of α-$(Al,Ga)_2O_3$ and κ-$(Al,Ga)_2O_3$. This is reflected in a less pronounced shift of the PL peak toward shorter wavelengths for the composite series in comparison with the monophase series, which corresponds to the actual Ga content in the garnet phase (y + z for the composite series, Table 1). Thus, the shift of the peak of the PL intensity by 18 nm for Al_2O_3–Ce:GAGG PCs with an increase in x to 3.0 corresponds to y + z = 1.48, i.e., is equivalent to the position for the sample in the Ce:GAGG series with x = 1.5.

Figure 8 shows the PL decay curves obtained by excitation at λ_{ex} = 460 nm and control of the Ce^{3+} PL peak at 560 nm. Except for Ce:GAGG samples with Ga contents of x = 2.5 and 3.0, the curves were described by one exponent $I(t) = A_0 + A_1 \cdot \exp^{\frac{-t}{\tau_1}}$. The lifetime ($\tau$) ranged from 61.3 to 53.8 ns and 60.0 to 57.1 ns for monophasic (x = 0.5–2.0) and composite (x = 0.5–3.0) phosphors, respectively (insets of Figs. 8(a) and 8(b)). The obtained values are in good agreement with those for Ce:GAGG ceramics with a Ga content (x) of 1.0 (58.9–60.2 ns) [16]. It is known that the increase in Ga^{3+} contributes to a decrease in crystal field cleavage in the structure of GAGG garnets [35,36]. The higher excitation band 5d shifts toward lower energies, and the lowest excitation and emission bands 5d shift toward higher energies. Thus, the process of returning Ce^{3+} ions from a high-energy (excited) state to their low-energy (ground) state is accelerated.

Quantum efficiency is calculated using the two-measurement method, which includes capturing the excitation and emission spectra of the PL without (first measurement) and with (second measurement) a sample in the sphere [37]. In particular, the corresponding calculation of the external quantum efficiency was carried out according to the equation $\eta(\mathrm{EQE}) = E_c/L_a$, where E_c–s is the integrated radiation spectrum of the sample, and L_a is the integrated excitation spectrum without a sample in the sphere. The η(EQE) values of Ce:GAGG and Al_2O_3–Ce:GAGG PCs varied in the ranges of 58%–64% and 55%–62%, respectively (which exceeds the known literature data for Ce:GAGG PCs [16]). The exception was the Ce:GAGG sample with the maximum Ga content, for which a decrease in the η(EQE) value to 28% was shown (insets of Figs. 8(a) and 8(b)).

It was found that an increase in the background noise level for Ce:GAGG with Ga content x = 2.5 and 3.0 indicated the manifestation of phosphorescence (Fig. 9). This phenomenon is associated with the presence of internal lattice defects that act as

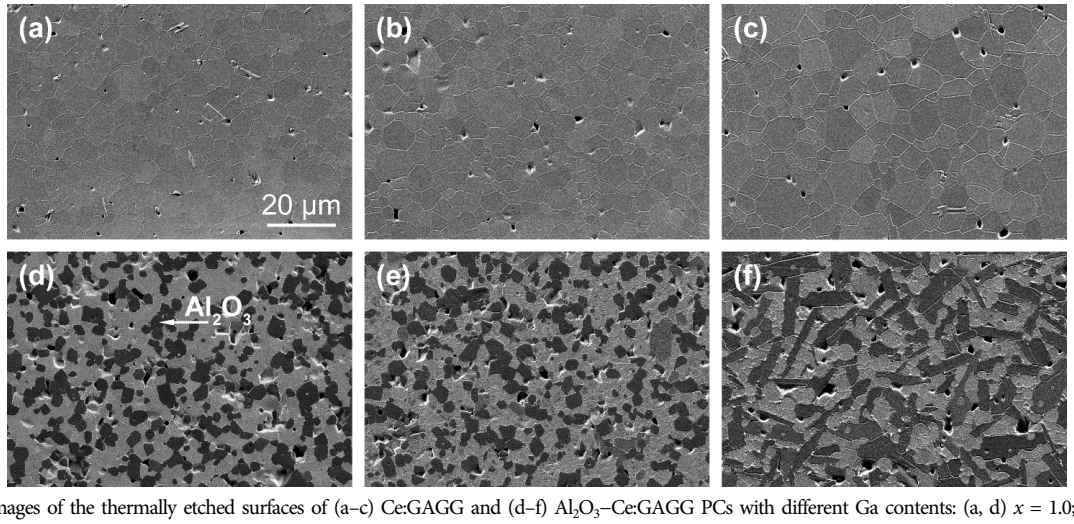

Fig. 5 SEM images of the thermally etched surfaces of (a–c) Ce:GAGG and (d–f) Al_2O_3–Ce:GAGG PCs with different Ga contents: (a, d) x = 1.0; (b, e) x = 2.0; and (c, f) x = 3.0.

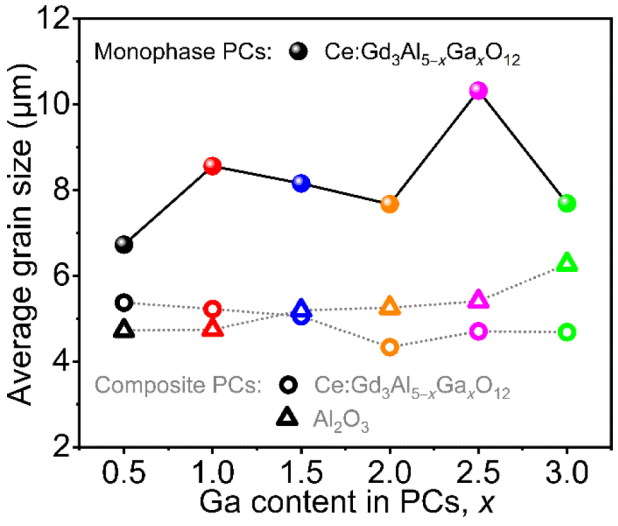

Fig. 6 Average grain sizes of constituent phases for Ce:GAGG and Al_2O_3–Ce:GAGG PCs with different Ga contents.

electronic traps of charge carriers, and it is undesirable for real-time lighting applications where quick decay is needed. The decay curves were described by an equation with two exponents $I(t) = A \cdot \exp^{\frac{-t}{\tau_1}} + B \cdot \exp^{\frac{-t}{\tau_2}} + C$, where A, B, and C are constants, and τ_1 and τ_2 are fast and slow decay components. The phosphor samples had a long afterglow – the values of τ_1 (τ_2) for compositions with x = 2.5 and 3.0 were 7060 (72,279) ms and 58,602 (393,327) ms, respectively. Given that the garnet solid solution phase in the Al_2O_3–Ce:GAGG composite series deviated from the nominal composition ($y + z << x$ and did not exceed 1.5), no decrease in lifetime below ~57 nm or transition to phosphorescence mode occurred in these samples (Fig. 8, Table 1).

The certification of the lighting characteristics of the phosphor series was carried out at a power density of blue LD of 1 W·mm^{-2} in the "reflection" mode (Fig. 10). Two bands were observed in the emission spectra centered at ~450 nm (blue LD excitation) and at 545–560 nm (yellow phosphor emission when blue light is excited) (Figs. 10(a) and 10(b)). The observed blueshift and narrowed FWHM (Fig. 7; insets in Figs. 10(a) and 10(b)) can affect color coordinates by raising the correlated color temperature (cooler, bluer light) and dropping the color rendering index due to reduced spectral coverage across visible wavelengths. However, the resulting LE, CCT, and Ra values for PCs will be set not only by the contribution of the crystal field splitting around Ce^{3+} activators but also by the Ce^{3+} density per unit volume, total transmittance, volume of light scattering centers, etc. Obviously, the observed disruption in the structural-phase state stability of PCs at high Ga amounts will also affect their luminescence performance (Figs. 3, 5, and 9). The most stable lighting characteristics were compositions with x = 0.5–1.5. In particular, for Al_2O_3–Ce:GAGG PCs, the values of LE, CCT, and CRI varied in the ranges of 123–145 lm·W^{-1}, 5400–6300 K, and 64–69, respectively (Fig. 10(d)). With similar phosphor thickness and input power, Zhao *et al.* [3] achieved LE values of 180 lm·W^{-1}, CCT 3800 K, and CRI 60 for 50 vol% Al_2O_3–Ce:GAGG PCs with x = 1. In turn, the measured CCT for monophase and composite PCs with x = 3.0 and x > 2.0, respectively, was excessively high (above 10,000 K), rendering devices based on these phosphor samples impractical for real-world applications.

As a comparison, the thermal conductivity of Ce:GAGG and Al_2O_3–Ce:GAGG PCs with x = 1.0 was measured over the

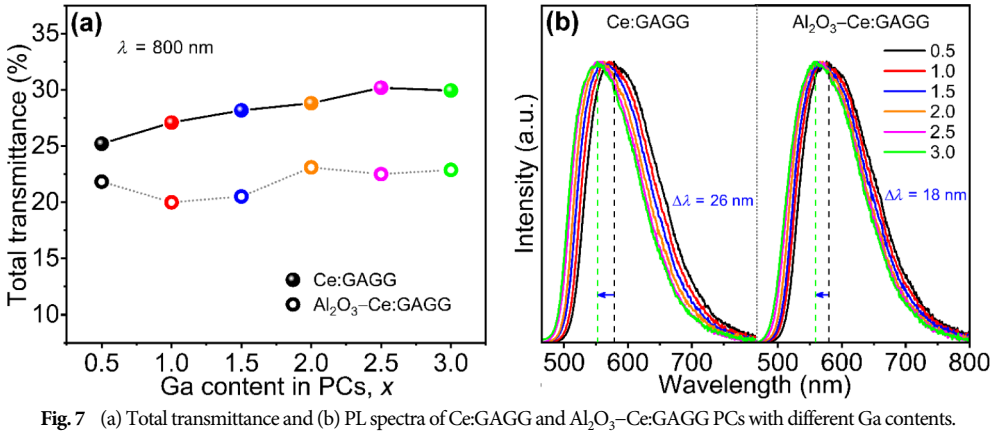

Fig. 7 (a) Total transmittance and (b) PL spectra of Ce:GAGG and Al_2O_3–Ce:GAGG PCs with different Ga contents.

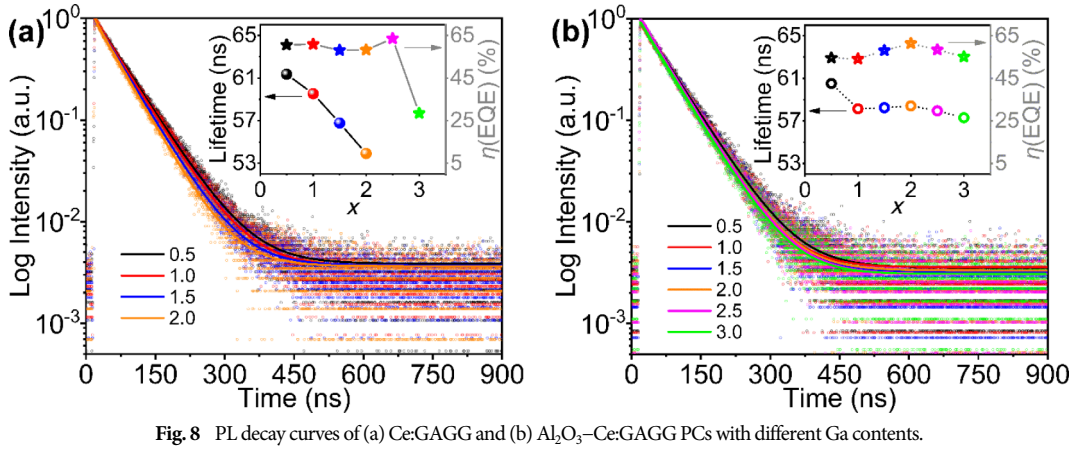

Fig. 8 PL decay curves of (a) Ce:GAGG and (b) Al_2O_3–Ce:GAGG PCs with different Ga contents.

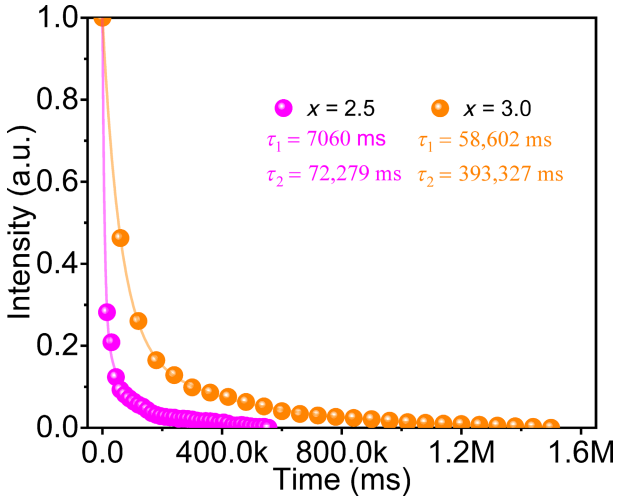

Fig. 9 Phosphorescence decay curves of Ce:GAGG PCs with Ga content x = 2.5 and 3.0.

temperature range from 25 to 225 °C. The obtained values for monophase and composite samples at RT were 9.0 and 6.9 $W \cdot m^{-1} \cdot K^{-1}$, respectively, which are lower than those of Ce:YAG (9.6 $W \cdot m^{-1} \cdot K^{-1}$) and Al_2O_3–Ce:YAG (12.5 $W \cdot m^{-1} \cdot K^{-1}$) PCs in the literature due to the many constituent elements and the complex structure of Ce:GAGG [38,39]. The temperature relations of the thermal conductivity for both samples had a similar appearance. As a result, the decrease in their values with an increase in temperature to 225°C was 31%±2%. One effective method to improve thermal conductivity in Ce:GAGG and Al_2O_3–Ce:GAGG PCs (in this case, optical uniformity) involves combined sintering techniques, particularly oxygen-atmosphere sintering followed by hot isostatic pressing treatment [3,9]. Finally, the obtained Al_2O_3–Ce:GAGG composite ceramics could be applicable as promising phosphor materials for high color rendering laser lighting.

4 Conclusions

A series of monophase Ce:GAGG and composite Al_2O_3–Ce:GAGG PCs with different Al_{5-x}/Ga_x ratios in nominal compositions (x = 0.5–3.0) were prepared in a pure oxygen atmosphere. The effects of Ga^{3+} substitution on their phase formation, microstructure, and luminescence properties were systematically investigated.

For Ce:GAGG systems, no additional phases were identified; the distribution of Ga between the octahedral $(Al/Ga)_2$ (0, 0, 0) and tetrahedral $(Al/Ga)_3$ (0.375, 0, 0.25) sites of the garnet phase and their influence on the lattice parameter were clarified according to the expression a[Å] = 12.1081 + 0.0517·Ga_{octa} + 0.0520·Ga_{tetra}. For Al_2O_3–Ce:GAGG systems, the exchange of Al and Ga elements between the garnet phases Ga(Al,Ga)G and $(Al,Ga)_2O_3$ was revealed, the transformation of $(Al,Ga)_2O_3$ from α- to a low-symmetric orthorhombic κ-modification was shown as $x \geq 2.0$ increased, and the proportion of the new κ-$(Al,Ga)_2O_3$ phase in the total amount of $(Al,Ga)_2O_3$ oxide was estimated.

The effect of Ga^{3+} substitution in Ce:GAGG on their grain structure was complex: a maximum was observed at x = 2.5 (10.3 μm), with an overall increase in average sizes in the series from 6.7 to 7.7 μm. The phase boundaries in the composite series were natural stoppers of intergranular diffusion: as the total amount of Ga in the system increased, the growth of alumina was

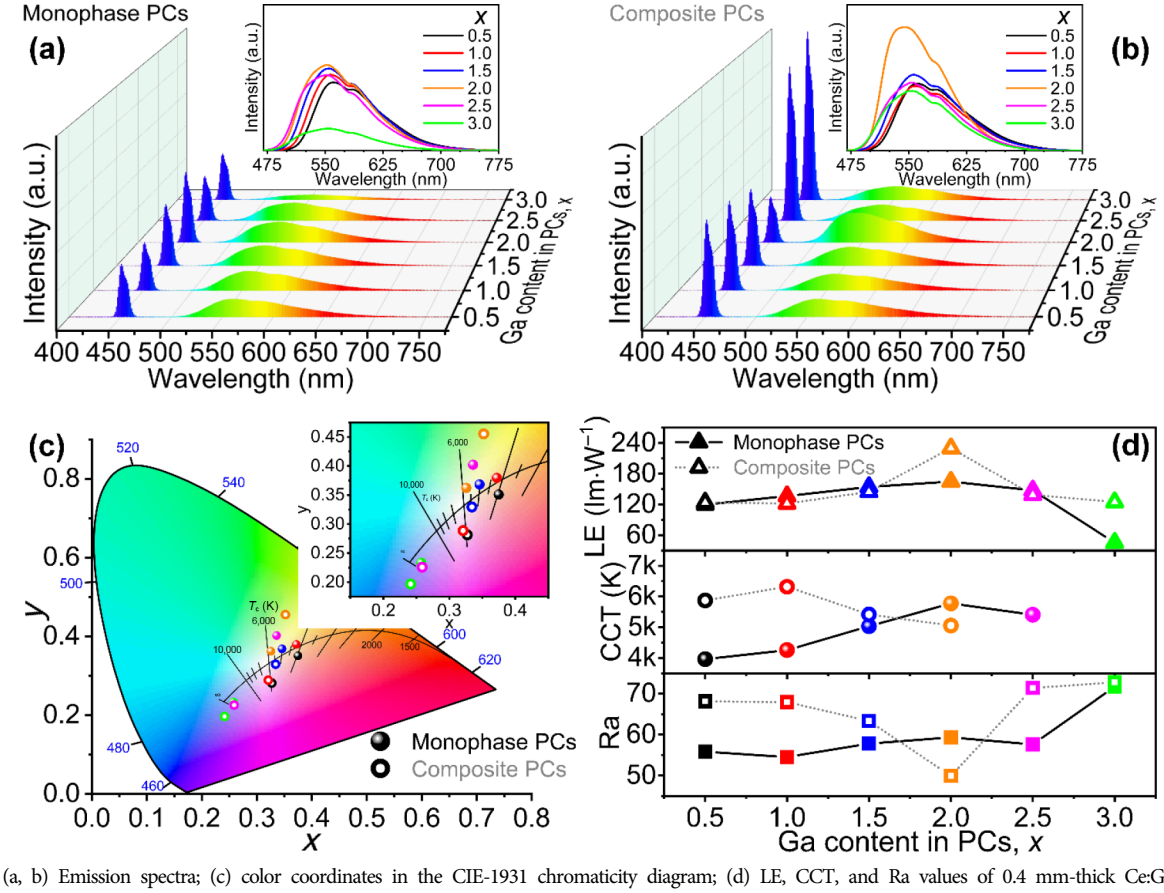

Fig. 10 (a, b) Emission spectra; (c) color coordinates in the CIE-1931 chromaticity diagram; (d) LE, CCT, and Ra values of 0.4 mm-thick Ce:GAGG and Al_2O_3–Ce:GAGG PCs with different Ga contents under excitation of a 1 $W \cdot mm^{-2}$ blue LD.

shown in the range from 4.7 to 6.3 μm, with a slight decrease for garnet from 5.4 to 4.7 μm. In addition, in Al_2O_3–Ce:GAGG at x = 3, intensive recrystallization of alumina took place with the formation of elongated grains and their partial melting and coalescence of pores. Obviously, the observed $(Al,Ga)_2O_3$ phase transition α → κ is a significant factor capable of causing these microstructural changes.

The formation of α-$(Al,Ga)_2O_3$ and κ-$(Al,Ga)_2O_3$ solid solutions partially offsets the contribution to the splitting of the crystalline field in the garnet structure due to the replacement of Al by larger Ga atoms. With increasing Ga content, the PL peak shifted toward shorter wavelengths for Ce:GAGG and Al_2O_3–Ce:GAGG PCs by ~26 and ~18 nm, respectively, with its narrowing by ~9 and ~3 nm. A phosphorescence phenomenon was found for monophasic Ce:GAGG compositions with x = 2.5 and 3.0—the values of τ_1 (τ_2) were 7060 (72,279) ms and 58,602 (39,3327) ms.

The luminous performance of PCs was tested under an input power density of 1 W·mm^{-2} blue LDs in reflection mode at λ_{ex} = 450 nm. It was shown that 0.4 mm-thick Al_2O_3–Ce:GAGG with x = 0.5–1.5 had an optimum CCT of 5400–6300 K, an LE of 123–145 lm·W^{-1}, and Ra of 69–64. The results indicate that the obtained composite ceramics can be used as promising phosphor converters for high color rendering laser lighting.

Acknowledgements

This work was supported by grants from the Ministry of Science and Higher Education of the Russian Federation (FEFU Program "PRIORITY 2030": Engineering, topic No. 24-03-2.05-0011) and the Russian Science Foundation (No. 25-73-10179; optimization of white LD performance based on the obtained PCs). Additionally, this work was partially supported by the National Key R&D Program of China (No. 2023YFB3506600), the Special Exchange Program of the Chinese Academy of Sciences (No. 121631GJHZ2024017TBJH), and the Chinese Academy of Sciences President's International Fellowship Initiative (No. 2024PVA0096).

Availability of data and materials

The data that support the findings of this study are available from the corresponding author upon reasonable request.

Competing interests

The authors have no competing interests to declare that are relevant to the content of this article. The author Jiang Li is the Associate Editor of this journal.

References

[1] König H, Lell A, Ali M, *et al.* Blue 450 nm high power semiconductor continuous wave laser bars exceeding rollover output power of 80 W. *Proc SPIE* 2018, **10514**: 1051402.

[2] Kuritzky LY, Speck JS. Lighting for the 21st century with laser diodes based on non-basal plane orientations of GaN. *MRS Commun* 2015, **5**: 463–473.

[3] Zhao HY, Xu J, Li JS, *et al.* Fabrication of Al_2O_3–GAGG:Ce composite ceramic phosphors with excellent color quality for high-power laser-driven lighting. *J Eur Ceram Soc* 2024, **44**: 373–382.

[4] Lin SS, Lin H, Huang QM, *et al.* Highly crystalline $Y_3Al_5O_{12}$:Ce^{3+} phosphor-in-glass film: A new composite color converter for next-generation high-brightness laser-driven lightings. *Laser Photon Rev* 2022, **16**: 2200523.

[5] Yao Q, Hu P, Sun P, *et al.* YAG:Ce^{3+} transparent ceramic phosphors brighten the next-generation laser-driven lighting. *Adv Mater* 2020, **32**: 1907888.

[6] Liao SX, Jin SL, Pang T, *et al.* Novel color converters for high brightness laser-driven projection display: Transparent ceramics–glass ceramics film composite. *Adv Funct Mater* 2024, **34**: 2307761.

[7] Yu ZK, Li JY, Zhao JZ, *et al.* High luminescence saturation $Y_3Al_5O_{12}$:Ce^{3+}-diamond composite color converter for high-brightness laser-driven white lighting. *Laser Photonics Rev* 2025, **19**: 2401124.

[8] Xi GY, Zhou ZZ, Li J, *et al.* Transparent composite ceramic@aluminum with ultra-high thermal conductivity for high-brightness laser-driven lighting. *Adv Funct Mater* 2024, **34**: 2401026.

[9] Kosyanov DY, Vornovskikh AA, Zavjalov AP, *et al.* Influence of HIP post-treatment on the microstructure and luminescent properties of SPSed Al_2O_3–Ce:YAG composite ceramics. *J Alloys Compd* 2025, **1010**: 178153.

[10] Li SX, Zhu QQ, Tang DM, *et al.* Al_2O_3–YAG:Ce composite phosphor ceramic: A thermally robust and efficient color converter for solid state laser lighting. *J Mater Chem C* 2016, **4**: 8648–8654.

[11] Liu ZH, Li SX, Huang YH, *et al.* The effect of the porosity on the Al_2O_3–YAG:Ce phosphor ceramic: Microstructure, luminescent efficiency, and luminous stability in laser-driven lighting. *J Alloys Compd* 2019, **785**: 125–130.

[12] Ma YL, Li XC, Wu L, *et al.* Preparation of $(Lu,Y)_3(Al,Sc,Cr)_2Al_3O_{12}$ phosphor ceramics with high thermal stability for near-infrared LED/LD. *J Adv Ceram* 2024, **13**: 354–363.

[13] Liu XC, Yang CC, Li YB, *et al.* High recorded color rendering performance of single-structured Ce,Mn:$Y_3(Al,Sc)_2Al_3O_{12}$ phosphor ceramics for high-power white LEDs/LDs. *J Adv Ceram* 2024, **13**: 810–820.

[14] Ma YL, Wang ZD, Pang T, *et al.* A cyan-green-emitting garnet-structured $Lu_{3-x}Sc_xAl_{2-y}Sc_yAl_{3-z}Sc_zO_{12}$:$Ce^{3+}$ phosphor ceramics towards high-color-quality laser-driven lighting. *Ceram Int* 2024, **50**: 21074–21082.

[15] Sun P, Hu P, Liu YF, *et al.* Broadband emissions from $Lu_2Mg_2Al_2Si_2O_{12}$:Ce^{3+} plate ceramic phosphors enable a high color-rendering index for laser-driven lighting. *J Mater Chem C* 2020, **8**: 1405–1412.

[16] Liu S, Sun P, Liu YF, *et al.* Warm white light with a high color-rendering index from a single $Gd_3Al_4GaO_{12}$:Ce^{3+} transparent ceramic for high-power LEDs and LDs. *ACS Appl Mater Interfaces* 2019, **11**: 2130–2139.

[17] Li JG, Sakka Y. Recent progress in advanced optical materials based on gadolinium aluminate garnet ($Gd_3Al_5O_{12}$). *Sci Technol Adv Mater* 2015, **16**: 014902.

[18] Li JK, Li JG, Zhang ZJ, *et al.* Effective lattice stabilization of gadolinium aluminate garnet (GdAG) via Lu^{3+}doping and development of highly efficient (Gd,Lu)AG:Eu^{3+} red phosphors. *Sci Technol Adv Mater* 2012, **13**: 035007.

[19] Chen XQ, Qin HM, Zhang Y, *et al.* Effects of Ga substitution for Al on the fabrication and optical properties of transparent Ce:GAGG-based ceramics. *J Eur Ceram Soc* 2017, **37**: 4109–4114.

[20] Hellstrom EE, Ray II RD, Zhang C. Preparation of gadolinium gallium garnet [$Gd_3Ga_5O_{12}$] by solid-state reaction of the oxides. *J Am Ceram Soc* 1989, **72**: 1376–1381.

[21] Liu P, Liu YF, Cui CE, *et al.* Enhanced luminescence and afterglow by heat-treatment in reducing atmosphere to synthesize the $Gd_3Al_2Ga_3O_{12}$:Ce^{3+} persistent phosphor for AC-LEDs. *J Alloys Compd* 2018, **731**: 389–396.

[22] Rodríguez-Carvajal J. Recent advances in magnetic structure determination by neutron powder diffraction. *Phys B Condens Matter* 1993, **192**: 55–69.

[23] Rodríguez-Carvajal J. Rietveld refinement from powder diffraction data. *Newsletter* 2001, **26**: 12–19.

[24] Vaitkus A, Merkys A, Sander T, *et al.* A workflow for deriving chemical entities from crystallographic data and its application to the Crystallography Open Database. *J Cheminform* 2023, **15**: 123.

[25] Vaitkus A, Merkys A, Gražulis S. Validation of the crystallography

open database using the crystallographic information framework. *J Appl Crystallogr* 2021, **54**: 661–672.
[26] Wurst JC, Nelson JA. Lineal intercept technique for measuring grain size in two-phase polycrystalline ceramics. *J Am Ceram Soc* 1972, **55**: 109.
[27] Lin YC, Bettinelli M, Sharma SK, *et al.* Unraveling the impact of different thermal quenching routes on the luminescence efficiency of the $Y_3Al_5O_{12}$:Ce^{3+}phosphor for white light emitting diodes. *J Mater Chem C* 2020, **8**: 14015–14027.
[28] Vornovskikh AA, Zavjalov AP, Shichalin OO, *et al.* The luminescence kinetics of Al_2O_3–Ce:YAG ceramic phosphors: Application of SR for correct investigations. In: Proceedings of the 2024 IEEE 25th International Conference of Young Professionals in Electron Devices and Materials, 2024: 860–865.
[29] Kosyanov DY, Vornovskikh AA, Shichalin OO, *et al.* Reactive SPS of Al_2O_3–RE:YAG (RE = Ce; Ce + Gd) composite ceramic phosphors. *J Adv Ceram* 2023, **12**: 1015–1032.
[30] Sackville Hamilton AC, Lampronti GI, Rowley SE, *et al.* Enhancement of the magnetocaloric effect driven by changes in the crystal structure of Al-doped GGG, $Gd_3Ga_{5-x}Al_xO_{12}$ ($0 \le x \le 5$). *J Phys: Condens Matter* 2014, **26**: 116001.
[31] Spassky D, Kozlova N, Zabelina E, *et al.* Influence of the Sc cation substituent on the structural properties and energy transfer processes in GAGG:Ce crystals. *CrystEngComm* 2020, **22**: 2621–2631.
[32] Nakatsuka A, Yoshiasa A, Yamanaka T. Cation distribution and crystal chemistry of $Y_3Al_{5-x}Ga_xO_{12}$ ($0 \le x \le 5$) garnet solid solutions. *Acta Crystallogr B Struct Sci* 1999, **55**: 266–272.
[33] Marezio M, Remeika JP, Dernier PD. Cation distribution in $Y_3Al_{5-c}Ga_cO_{12}$ garnet. *Acta Crystallogr Sect B* 1968, **24**: 1670–1674.
[34] Cora I, Mezzadri F, Boschi F, *et al.* The real structure of ε-Ga_2O_3 and its relation to κ-phase. *CrystEngComm* 2017, **19**: 1509–1516.
[35] Ueda J, Tanabe S. (INVITED) Review of luminescent properties of Ce^{3+}-doped garnet phosphors: New insight into the effect of crystal and electronic structure. *Opt Mater X* 2019, **1**: 100018.
[36] Ogiegło JM, Katelnikovas A, Zych A, *et al.* Luminescence and luminescence quenching in $Gd_3(Ga,Al)_5O_{12}$ scintillators doped with Ce^{3+}. *J Phys Chem A* 2013, **117**: 2479–2484.
[37] Leyre S, Coutino-Gonzalez E, Joos JJ, *et al.* Absolute determination of photoluminescence quantum efficiency using an integrating sphere setup. *Rev Sci Instrum* 2014, **85**: 123115.
[38] Wen B, Zhang DF, Jiang B, *et al.* Thermal conductivity of Ce^{3+} doped $(Y,Gd)_3Al_5O_{12}$ ceramic phosphor. *J Lumin* 2020, **221**: 116886.
[39] Xu M, Chang J, Wang J, *et al.* Al_2O_3–YAG:Ce composite ceramics for high-brightness lighting. *Opt Express* 2019, **27**: 872.